An exact Riemann solver for one-dimensional multi-material elastic-plastic flows with Mie-Grüneisen equation of state

Li Liu[1], Jun-bo Cheng [1,*]

July 7, 2019

Abstract

In this paper, we present exact Riemann solvers for the Riemann problem and the half Riemann problem, respectively, for one-dimensional multi-material elastic-plastic flows with the Mie-Grüneisen equation of state(EOS), hypo-elastic constitutive model and the von Mises' yielding condition. We first analyze the Jacobian matrixes in both elastic and plastic states, and then build relations between different variables across different type of waves. Based on these formulations, an exact Riemann solver is constructed with totally thirty-six possible cases of wave structures. Although Gao and Liu[8] also developed the exact Riemann solver for 1D elastic plastic flows, but the EOS they used is very simple. Moreover, the exact Riemann solver developed by them may result in wrong solutions when the initial material is in the plastic state, which has been proven in one of our tests. Comparing with the exact Riemann solver developed by Gao and Liu, our exact Riemann solver uses a more complex EOS and overcomes these mistakes. A large number of tests prove the rightness of our exact Riemann solver. Moreover, an exact Riemann solver is also deduced for the half Riemann problem and its validity is tested by two examples.

1 Introduction

In this paper, an exact Riemann solver is built for one-dimensional multi-material elastic-plastic flows with the Mie-Grüneisen EOS, hypo-elastic constitutive model [1] and the von Mises' yielding condition.

The elastic-plastic flow is used to describe the deformation process of solid materials under strong dynamics loading, such as explosive or high-speed impact. The simulation of elastic-plastic flows has important application backgrounds, especially in the Implosion Dynamics weapon and Inertial Confine Fusion (ICF). The first try of simulating the elastic-plastic flows was given by Wilkins [1] in 1960s.

In the development history of hydrodynamic numerical methods, the exact Riemann solver has played a very important role as it not only can give a guide and reference to the construction of approximate Riemann solvers, but also can be used to determine the convergence and stability of numerical schemes. However, building the exact Riemann solver for 1D elastic-plastic flows is not that easy. Comparing with the governing equations system of 1D pure fluids, for 1D elastic-plastic flows, there are two more equations: a non-conservative constitutive equation and the von Mises yielding condition. The non-conservative character of the constitutive equation increases the difficulty in constructing Riemann solvers, while the von Mises yielding condition may lead to more non-linear waves in the wave structure of Riemann solvers. Moreover, in a general way, the equation of state(EOS) for solid materials is more complex than that for pure fluids, which directly increases the difficulty in solving the Riemann problem.

For the elastic-plastic flow with the hypo-elastic constitutive model and the von Mises' yielding condition, some approximate Riemann solvers[2, 3, 4, 5] have been developed recently. However, for the exact Riemann solver, the research is relatively few, and focuses mainly on the problem with relatively simple constitutive models and relatively simple EOSs. For example, Garaizar [6] and Miller [7] introduced an exact Riemann solver for elastic or hyper-elastic materials, Gao and Liu [8, 9] firstly considered the yielding effect and developed an exact elastic-perfectly plastic solid Riemann solver. But there are two shortcomings in their works. Firstly, the EOS used by them is very simple: in the elastic state, the material derivative of pressure is the linear function of the strain rate, which means the energy equation is not necessary in the elastic state; in the plastic state, a linear "stiffened-gas" EOS was used. Secondly, unloading (for example, an expanding

process to a compressed yielding material) and reloading processes are not considered in the construction of their Riemann solvers. This may leads to wrong solutions as the unloading and reloading are very common in the real computing cases, shown in our 5th numerical example. In fact, according to the relations in the governing equations, even if the initial material reaches the elastic limit and in a plastic state, after an unloading process, the material may change back to an elastic state and then may re-change to a plastic state by a reloading process.

In this paper, we want to construct an exact Riemann solver for the system of 1D elastic-plastic flows with the Mie-Grüneisen EOS, the hypo-elastic constitutive model and the von Mises' yielding condition. As every knows, the Mie-Grüneisen EOS is complex and is used widely in many engineering problems, which makes the energy equation must be included in the system of elastic-plastic flows and so we have to use some special methods to resolve the rarefaction wave. Otherwise, we analyse the Jacobian matrix and find, in the wave structures of Riemann solvers, there may be three to five waves, including one contact wave and other two to four non-linear waves. These nonlinear waves may be elastic shock waves, elastic rarefaction waves, plastic shock waves or plastic rarefaction waves. Moreover, elastic wave always runs faster than the followed plastic wave. So there are thirty-six possible cases of the wave structures in the Riemann solver. Besides, both the changing from elastic to plastic (loading or reloading) and the converse changing from plastic to elastic(unloading) are considered in the Riemann problem.

This paper is organized as follows. In section 2, we introduce the governing equations to be studied. In section 3, the Riemann problem and the relations for every wave type (contact wave, shock wave and rarefaction wave) are derived. Then, the exact Riemann solver is given in section 4. The half Riemann problem and its solver is introduced in section 5. Some numerical examples are presented to validate the method in section 6. Conclusions are shown in section 7.

2 Governing equations

In this paper, the elastic energy is not included in the total energy. The exclution of the elastic energy is usual for practical engineering problems [10] and is different from that in Ref.[2].

2.1 Motion equations

For a continuous one-dimensional homogeneous solid, the motion equations in the differential form are

$$\partial_t \mathbf{U} + \partial_x \boldsymbol{F}(\mathbf{U}) = 0,\ x \in\ \Omega \subset \mathbf{R},\ t > 0,$$

where

$$\mathbf{U} = \begin{bmatrix} \rho \\ \rho u \\ \rho E \end{bmatrix}, \quad \mathbf{F} = \begin{bmatrix} \rho u \\ \rho u^2 - \sigma \\ (\rho E - \sigma) u \end{bmatrix}, \tag{2.1}$$

ρ, u, σ and E are the density, velocity in $x-$direction, Cauchy stress and total energy per unit volume, respectively, E has the relation with the specific internal energy e as

$$E = e + \frac{1}{2}u^2, \tag{2.2}$$

$$\sigma = -p + s_{xx}, \tag{2.3}$$

where p and s_{xx} denote the hydrostatic pressure and the deviatoric stress in the $x-$ direction, respectively.

2.2 The equation of state (EOS)

The relation of the pressure with the density and the specific internal energy is gotten from the equation of state (EOS). In this paper, we consider the Mie-Grüneisen EOS,

$$p(\rho, e) = \rho_0 a_0^2 f(\eta) + \rho_0 \Gamma_0 e, \tag{2.4}$$

where $f(\eta) = \frac{(\eta-1)(\eta-\Gamma_0(\eta-1)/2)}{(\eta-s(\eta-1))^2}$, $\eta = \frac{\rho}{\rho_0}$, ρ_0, a_0, s and Γ_0 are constant parameters of the Mie-Grüneisen EOS.

2.3 The constitutive relation

Hooke's law is used here to describe the relationship between the deviatoric stress and the strain,

$$\dot{s}_{xx} = 2\mu\left(\dot{\varepsilon}_x - \frac{1}{3}\frac{\dot{V}}{V}\right), \tag{2.5}$$

where μ is the shear modulus, V is the volume, and the dot means the material time derivative,

$$\dot{()} = \frac{\partial()}{\partial t} + u\frac{\partial()}{\partial t}, \tag{2.6}$$

and

$$\dot{\varepsilon}_x = \frac{\partial u}{\partial x}, \quad \frac{\dot{V}}{V} = \frac{\partial u}{\partial x}. \tag{2.7}$$

By using Eq.(2.7), Eq.(2.5) can be rewritten as

$$\frac{\partial s_{xx}}{\partial t} + u\frac{\partial s_{xx}}{\partial t} = \frac{4}{3}\mu\frac{\partial u}{\partial x}. \tag{2.8}$$

2.4 The yielding condition

The Von Mises' yielding condition is used here to describe the elastic limit. In one spatial dimension, the von Mises' yielding criterion is given by

$$|s_{xx}| \leq \frac{2}{3}Y_0, \tag{2.9}$$

where Y_0 is the yield strength of the material in simple tensions.

3 The Riemann problem

The Riemann problem for 1D time dependent elastic-plastic equations is given as follows:

$$\begin{cases} \partial_t\rho + \partial_x(\rho u) = 0, \\ \partial_t(\rho u) + \partial_x(\rho u^2 + p - s_{xx}) = 0, \\ \partial_t(\rho E) + \partial_x\left[(\rho E + p - s_{xx})u\right] = 0, \\ \partial_t s_{xx} + u\partial_x s_{xx} - \dfrac{4}{3}\partial_x u = 0, \\ |s_{xx}| \leq \dfrac{2}{3}Y_0, \\ Q(x, t=0) = \begin{cases} Q_L, \text{ if } x < 0, \\ Q_R, \text{ if } x \geq 0, \end{cases} \end{cases} \tag{3.1}$$

where $Q = (\rho, \rho u, \rho E, s_{xx})^T$.

The above equations are just for the elastic status of the solid material. If the materials are in the plastic state, the above equations can be simplified and the jacobian matrix and sonic velocity are different, correspondingly. We will discuss them separately.

3.1 Elastic state

3.1.1 Jacobian matrix in elastic regions

For the Mie-Grüneisen EOS, if the material is not yielding,

$$|s_{xx}| < \frac{2}{3}Y_0, \tag{3.2}$$

the system (3.1) can be written as

$$\partial_t \mathbf{Q} + \mathbf{J}_e(\mathbf{Q})\partial_x \mathbf{Q} = 0, \tag{3.3}$$

where $Q = (\rho, \rho u, \rho E, s_{xx})$, and the Jacobian matrix is

$$\mathbf{J}_e(Q) = \begin{bmatrix} 0 & 1 & 0 & 0 \\ -u^2 + \frac{\partial p}{\partial \rho} + \Gamma(\frac{u^2}{2} - e) & u(2-\Gamma) & \Gamma & -1 \\ (\Gamma(\frac{u^2}{2} - e) - e - \frac{u^2}{2} + \frac{\sigma}{\rho} + \frac{\partial p}{\partial \rho})u & -\Gamma u^2 - \frac{\sigma}{\rho} + \frac{u^2}{2} + e & (1+\Gamma)u & -u \\ \frac{4}{3}\mu\frac{u}{\rho} & -\frac{4}{3}\mu\frac{1}{\rho} & 0 & u \end{bmatrix}, \tag{3.4}$$

where $\Gamma = \frac{\Gamma_0 \rho_0}{\rho}$.

The eigenvalues of $\mathbf{J}_e(\mathbf{Q})$ are given as

$$\lambda_1 = \lambda_2 = u, \quad \lambda_3 = u - c_e, \quad \lambda_4 = u + c_e, \tag{3.5}$$

where c_e means the sonic speed of the solid in the elastic state,

$$\begin{cases} c_e = \sqrt{a^2 - \dfrac{\rho_0}{\rho^2}\Gamma_0 s_{xx} + \dfrac{4}{3}\dfrac{\mu}{\rho}}, \\ a^2 = \dfrac{\partial p}{\partial \rho} + \dfrac{p}{\rho^2}\dfrac{\partial p}{\partial e} = a_0^2 \dfrac{\partial f}{\partial \eta} + \dfrac{p}{\rho^2}\rho_0\Gamma_0. \end{cases} \tag{3.6}$$

Corresponding right eigenvectors are

$$r_1 = \begin{bmatrix} \frac{1}{b_1} \\ \frac{u}{b_1} \\ 0 \\ 1 \end{bmatrix}, \quad r_2 = \begin{bmatrix} -\frac{\Gamma}{b_1} \\ -\frac{\Gamma u}{b_1} \\ 1 \\ 0 \end{bmatrix}, \quad r_3 = \frac{1}{\phi^2}\begin{bmatrix} 1 \\ u - c_e \\ h - uc_e \\ \phi^2 \end{bmatrix}, \quad r_4 = \frac{1}{\phi^2}\begin{bmatrix} 1 \\ u + c_e \\ h + uc_e \\ \phi^2 \end{bmatrix}, \tag{3.7}$$

where

$$b_1 = \frac{\partial p}{\partial \rho} - \Gamma E, \quad h = E + \frac{p - s_{xx}}{\rho}, \tag{3.8}$$

and

$$\phi^2 = a^2 - \frac{\rho_0}{\rho^2}\Gamma_0 s_{xx} - c_e^2 = -\frac{4\mu}{3}\frac{1}{\rho}. \tag{3.9}$$

3.1.2 A relation between ρ and s_{xx}

Thanks to (2.6), equations of the density and the deviatoric stress in Eq.(3.1) can be written as

$$\frac{\partial u}{\partial x} = -\frac{1}{\rho}\frac{d\rho}{dt}, \tag{3.10}$$

and

$$\frac{ds_{xx}}{dt} = \frac{4}{3}\mu\frac{\partial u}{\partial x}. \tag{3.11}$$

Substituting (3.10) into (3.11) yields

$$\frac{ds_{xx}}{dt} = -\frac{4}{3}\mu\frac{1}{\rho}\frac{d\rho}{dt}. \tag{3.12}$$

Integrating the above equation from the data in front of a wave to the data behind the wave and performing some simple algebraic manipulations, one can get

$$s_{xx} + \frac{4}{3}\mu \ln(\rho) = \text{constant} \tag{3.13}$$

This relation always hold in the elastic state.

3.1.3 Relations across the contact wave

For a system without molecular diffusion, there is no materials convecting across the contact wave or interface, so the velocities on two sides of the discontinuity are always equal. This can also be verified by eigenvectors in Eq.(3.7) and Eq.(3.62).

Using $\mathbf{Q}_L^*$ and $\mathbf{Q}_R^*$ to denote the two data states connected the contact wave, where $\mathbf{Q} = (\rho, u, p, s_{xx})$.

Thanks to Eq.(3.7), for the λ_1-wave we have

$$\frac{d\rho}{\frac{1}{b_1}} = \frac{d\rho u}{\frac{u}{b_1}} = \frac{d\rho E}{0} = \frac{ds_{xx}}{1}. \tag{3.14}$$

From above equations, we can easily deduce that

$$du = 0, \quad d(s_{xx} - p) = 0, \tag{3.15}$$

which means

$$u_L^* = u_R^*, \tag{3.16}$$

and

$$\sigma_{x,L}^* = \sigma_{x,R}^*, \tag{3.17}$$

where $()_L^*$ and $()_R^*$ denote $()$ in the region of $\mathbf{Q}_L^*$ and $\mathbf{Q}_R^*$, respectively. Here we do not show the details of the derivation for a simple presentation.

Similarly, for the λ_2-wave one has

$$\frac{d\rho}{\frac{-\Gamma}{b_1}} = \frac{d\rho u}{\frac{-u\Gamma}{b_1}} = \frac{d\rho E}{1} = \frac{ds_{xx}}{0}. \tag{3.18}$$

From the above equations, we can easily deduce that

$$du = 0, \quad dp = 0, \quad ds_{xx} = 0, \tag{3.19}$$

which means

$$u_L^* = u_R^*, \tag{3.20}$$

$$p_L^* = p_R^*, \quad s_{xx,L}^* = s_{xx,R}^*. \tag{3.21}$$

From Eq.(3.21), we get that

$$\sigma_{x,L}^* = \sigma_{x,R}^*. \tag{3.22}$$

At last, for the λ_1 and λ_2 waves, one can find that the following two relations always hold:

$$u_L^* = u_R^*, \quad \sigma_{x,L}^* = \sigma_{x,R}^*. \tag{3.23}$$

For convenience, we define

$$s^* = u_L^* = u_R^*. \tag{3.24}$$

where s^* denotes the velocity of the contact wave.

3.1.4 Relations across rarefaction waves

Left-going rarefaction wave Across the left wave associated with λ_3-wave, $(\lambda_3 = u - c_e)$, we have

$$\frac{d\rho}{1} = \frac{d(\rho u)}{u - c_e} = \frac{d(\rho E)}{h - uc_e} = \frac{ds_{xx}}{-\frac{4\mu}{3}\frac{1}{\rho}}. \tag{3.25}$$

which leads to

$$\mathrm{d}u = -\frac{c_e}{\rho}\mathrm{d}\rho, \tag{3.26}$$

$$\mathrm{d}E = -\frac{\sigma + \rho u c_e}{\rho^2} d\rho, \tag{3.27}$$

$$\mathrm{d}s_{xx} = -\frac{4}{3}\frac{\mu}{\rho} d\rho. \tag{3.28}$$

Using (2.4), one can get

$$dE = de + udu. \tag{3.29}$$

Substituting (3.26) and (3.27) into the above equation yields

$$de = -\frac{\sigma}{\rho^2}d\rho = \frac{p - s_{xx}}{\rho^2}d\rho. \tag{3.30}$$

Thanks to (2.4), one can get

$$dp = \frac{\partial p}{\partial \rho}d\rho + \frac{\partial p}{\partial e}de = a_0^2\frac{\partial f}{\partial \eta}d\rho + \rho_0\Gamma_0 de, \tag{3.31}$$

Substituting (3.30) into the above equation yields

$$dp = \left(a_0^2\frac{\partial f}{\partial \eta} + \frac{p}{\rho^2}\rho_0\Gamma_0 - \frac{\rho_0}{\rho^2}\Gamma_0 s_{xx}\right)d\rho. \tag{3.32}$$

The above equation can be rewritten as a differential equation of $p(\rho)$

$$p'(\rho) - \lambda\frac{p}{\rho^2} = f_2(\rho), \tag{3.33}$$

where

$$\lambda = \rho_0\Gamma_0 \quad f_2(\rho) = a_0^2\frac{\partial f}{\partial \eta} - \lambda\frac{s_{xx}(\rho)}{\rho^2}. \tag{3.34}$$

By integrating (3.33) across the left rarefaction wave, the pressure can be solved out as

$$pe^{\frac{\lambda}{\rho}} - \int f_2(\rho)e^{\frac{\lambda}{\rho}}d\rho = \text{constant}. \tag{3.35}$$

Integrating (3.26) across the left rarefaction wave yields

$$u + \int \frac{c_e}{\rho}d\rho = \text{constant}. \tag{3.36}$$

Right-going rarefaction wave

Across the right wave associated with λ_4-wave, $(\lambda_3 = u + c_e)$, we have

$$\frac{d\rho}{1} = \frac{d(\rho u)}{u + c_e} = \frac{d(\rho E)}{h + uc_e} = \frac{ds_{xx}}{-\frac{4\mu}{3}\frac{1}{\rho}}. \tag{3.37}$$

which leads to

$$\mathrm{d}u = \frac{c_e}{\rho}\mathrm{d}\rho, \tag{3.38}$$

$$\mathrm{d}E = -\frac{\sigma + \rho u c_e}{\rho^2}d\rho, \tag{3.39}$$

$$\mathrm{d}s_{xx} = -\frac{4}{3}\frac{\mu}{\rho}d\rho. \tag{3.40}$$

By using the same method, one can get

$$pe^{\frac{\lambda}{\rho}} - \int f_2(\rho)e^{\frac{\lambda}{\rho}}d\rho = \text{constant}. \tag{3.41}$$

$$u - \int \frac{c_e}{\rho}d\rho = \text{constant}. \tag{3.42}$$

3.1.5 Relations across shock waves

Now we consider a shock wave moving with the speed of s. The data in front of the shock is $(\rho_1, u_1, p_1, s_{xx1})$ and that after the shock is $(\rho_2, u_2, p_2, s_{xx2})$.

We transform the equations to a frame of reference moving with the shock and the Rankine-Hugoniot Conditions give

$$\rho_2(u_2 - s) = \rho_1(u_1 - s), \tag{3.43}$$

$$\rho_2 u_2(u_2 - s) = \rho_1 u_1(u_1 - s) + \sigma_2 - \sigma_1, \tag{3.44}$$

$$\rho_2 E_2(u_2 - s) = \rho_1 E_1(u_1 - s) + \sigma_2 u_2 - \sigma_1 u_1. \tag{3.45}$$

Substituting (3.43) into (3.44) yields

$$\rho_1(u_2 - u_1)(u_1 - s) = \sigma_2 - \sigma_1. \tag{3.46}$$

From (3.43), one has

$$u_1 - s = \frac{(u_1 - u_2)\rho_2}{\rho_2 - \rho_1}, \tag{3.47}$$

then subtituting it into (3.46) yields

$$-t(u_2 - u_1)^2 = \sigma_2 - \sigma_1, \tag{3.48}$$

where $t = \frac{\rho_1\rho_2}{\rho_2 - \rho_1}$.

By using the same methods for (3.48), (3.45) can be written as

$$t(u_1 - u_2)(E_2 - E_1) = \sigma_2 u_2 - \sigma_1 u_1. \tag{3.49}$$

Because of $E = e + \frac{1}{2}u^2$, we can get

$$e_2 - e_1 = -\frac{\sigma_1 + \sigma_2}{2t}. \tag{3.50}$$

Using the EOS of Mie-Grüneisen (2.4), can get

$$e = c_0 p - c_1 f(\rho/\rho_0), \tag{3.51}$$

where $c_0 = \frac{1}{\rho_0\Gamma_0}$ and $c_1 = \frac{a_0^2}{\Gamma_0}$. Put the above equation into (3.50), we can solve the pressure p_2 out as a function of ρ_2.

$$p_2 = \frac{2t(c_1 f(\rho_2/\rho_0) + e_1) - (\sigma_1 + s_{xx2})}{2tc_0 - 1}. \tag{3.52}$$

Thanks to (3.13), s_{xx2} can be written as

$$s_{xx2} = s_{xx1} - \frac{4}{3}\mu \ln(\frac{\rho_2}{\rho_1}). \tag{3.53}$$

Then, the Cauchy stress can be written as

$$\sigma_2 = -p_2 + s_{xx2}. \tag{3.54}$$

Then we can use (3.48) to solve the velocity after the shock

$$u_2 = \begin{cases} u_1 - \sqrt{\dfrac{\sigma_1 - \sigma_2}{t}} & \text{Left-going,} \\ u_1 + \sqrt{\dfrac{\sigma_1 - \sigma_2}{t}} & \text{Right-going.} \end{cases} \tag{3.55}$$

And the shock speed is given as

$$s = \frac{\rho_2 u_2 - \rho_1 u_1}{\rho_2 - \rho_1}. \tag{3.56}$$

By the above deductions for the moving shock wave, we can find that, if the density after the shock is known, all the data after the shock can be solved out.

3.2 Plastic state

When the material is yielding,

$$|s_{xx}| = \frac{2}{3}Y_0, \tag{3.57}$$

the equations of Riemann problem can be written as

$$\begin{cases} \partial_t \rho + \partial_x(\rho u) = 0, \\ \partial_t(\rho u) + \partial_x(\rho u^2 + p - s_{xx}) = 0, \\ \partial_t(\rho E) + \partial_x\left[(\rho E + p - s_{xx})u\right] = 0, \\ |s_{xx}| = \frac{2}{3}Y_0, \\ U(x, t=0) = \begin{cases} U_L, \text{ if } x < 0, \\ U_R, \text{ if } x \geq 0, \end{cases} \end{cases} \tag{3.58}$$

where $\mathbf{U} = (\rho, \rho u, \rho E)$.

3.2.1 Jacobian matrix in plastic regions

Motion equations of (3.58) can be written as

$$\partial_t \mathbf{U} + \mathbf{J}_p(\mathbf{U})\partial_x \mathbf{U} = 0, \tag{3.59}$$

where the Jacobian matrix is

$$\mathbf{J}_p(\mathbf{U}) = \begin{bmatrix} 0 & 1 & 0 \\ -u^2 + \frac{\partial p}{\partial \rho} + \Gamma(\frac{u^2}{2} - e) & u(2-\Gamma) & \Gamma \\ (\Gamma(\frac{u^2}{2} - e) - e - \frac{u^2}{2} + \frac{\sigma}{\rho} + \frac{\partial p}{\partial \rho})u + \frac{u^2}{2} & -\Gamma u^2 - \frac{\sigma}{\rho} + e & (1+\Gamma)u \end{bmatrix}. \tag{3.60}$$

Eigenvalues of $\mathbf{J}_p(\mathbf{Q})$ are given as

$$\lambda_1 = u, \quad \lambda_2 = u - c_p, \quad \lambda_3 = u + c_p,$$

where

$$c_p = \sqrt{a^2 - \frac{\rho_0}{\rho^2}\Gamma_0 s_{xx}}. \tag{3.61}$$

The corresponding right eigenvectors are

$$r_1 = \begin{bmatrix} -\frac{\Gamma}{b_1} \\ -\frac{\Gamma u}{b_1} \\ 1 \end{bmatrix}, \quad r_2 = \frac{1}{h - uc_p}\begin{bmatrix} 1 \\ u - c_p \\ h - uc_p \end{bmatrix}, \quad r_3 = \frac{1}{h + uc_p}\begin{bmatrix} 1 \\ u + c_p \\ h + uc_p \end{bmatrix}. \tag{3.62}$$

Comparing Eq.(3.6) with Eq.(3.61), we notice that the sonic speed is not continuous between the states of elastic and plastic. As the shear modulus μ is always positive, so the elastic wave runs always faster than the plastic wave.

3.2.2 Relations across the contact wave

According to the eigenvectors in Eq.(3.62), for the λ_1-wave ($\lambda_1 = u$), we have

$$\frac{d\rho}{\frac{-\Gamma}{b_1}} = \frac{d(\rho u)}{\frac{-u\Gamma}{b_1}} = \frac{d(\rho E)}{1}. \tag{3.63}$$

From the above equations, we can easily deduce that

$$du = 0, \quad dp = 0, \tag{3.64}$$

which means that

$$u_L^* = u_R^*, \quad p_L^* = p_R^*. \tag{3.65}$$

Because $s_{xxL}^* = s_{xxR}^*$, thanks to (2.3), one can get

$$\sigma_L^* = \sigma_R^*. \tag{3.66}$$

For convenience, we define

$$s^* = u_L^* = u_R^*. \tag{3.67}$$

3.2.3 Relations across rarefaction waves

Left-going rarefaction wave Across the left wave associated with λ_2-wave, ($\lambda_2 = u - c_p$), we have

$$\frac{d\rho}{1} = \frac{d(\rho u)}{u - c_p} = \frac{d(\rho E)}{h - uc_p}. \tag{3.68}$$

Samilar to section 3.1.4, we can get the relations

$$pe^{\frac{\lambda}{\rho}} - \int f_2(\rho) e^{\frac{\lambda}{\rho}} d\rho = \text{constant}. \tag{3.69}$$

and

$$u + \int \frac{c_p}{\rho} d\rho = \text{constant}. \tag{3.70}$$

Right-going rarefaction wave Across the right wave associated with λ_3-wave, ($\lambda_3 = u + c_e$), we have

$$\frac{d\rho}{1} = \frac{d(\rho u)}{u + c_p} = \frac{d(\rho E)}{h + uc_p}. \tag{3.71}$$

We can get similar relations as the left-going wave as

$$pe^{\frac{\lambda}{\rho}} - \int f_2(\rho) e^{\frac{\lambda}{\rho}} d\rho = \text{constant}. \tag{3.72}$$

$$u - \int \frac{c_p}{\rho} d\rho = \text{constant}. \tag{3.73}$$

3.2.4 Relations across a shock wave

By using the same deducing process as Section 3.1.5, we can get the states after the shock wave as

$$s_{xx2} = s_{xx1}, \tag{3.74}$$

$$p_2 = \frac{2t(c_1 f(\rho_2/\rho_0) + e_1) - (\sigma_1 + s_{xx2})}{2tc_0 - 1}, \tag{3.75}$$

where $c_0 = \frac{1}{\rho_0 \Gamma_0}$, $c_1 = \frac{a_0^2}{\Gamma_0}$, $\sigma_2 = -p_2 + s_{xx2}$,

$$u_2 = \begin{cases} u_1 - \sqrt{\dfrac{\sigma_1 - \sigma_2}{t}} & \text{Left-going,} \\ u_1 + \sqrt{\dfrac{\sigma_1 - \sigma_2}{t}} & \text{Right-going.} \end{cases} \tag{3.76}$$

And the shock speed is given as

$$s = \frac{\rho_2 u_2 - \rho_1 u_1}{\rho_2 - \rho_1}. \tag{3.77}$$

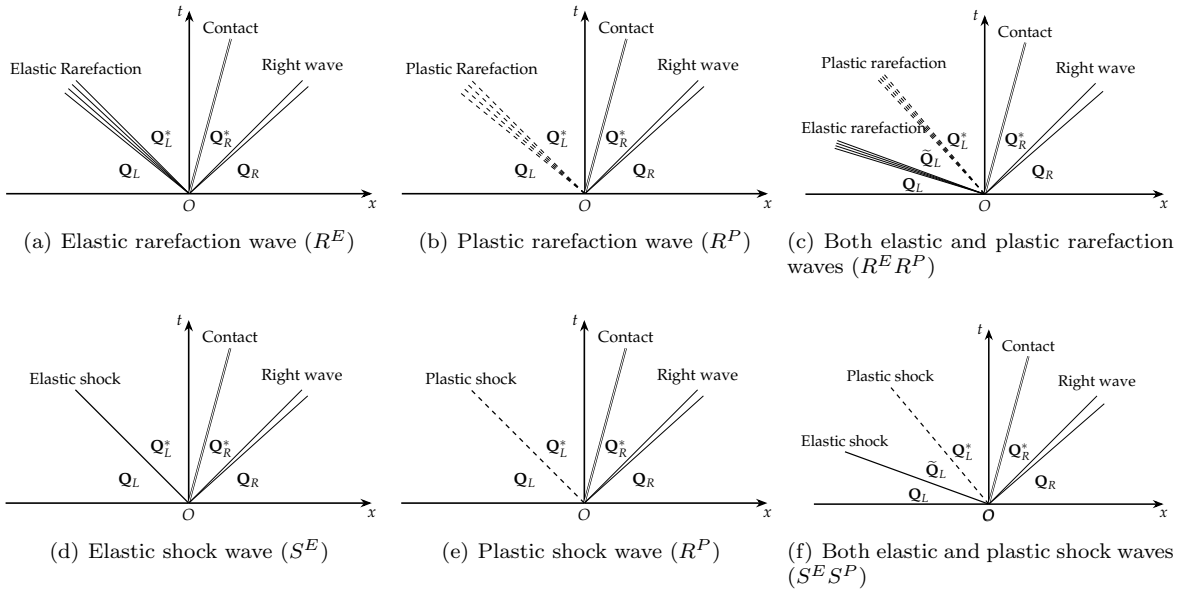

(a) Elastic rarefaction wave (R^E)

(b) Plastic rarefaction wave (R^P)

(c) Both elastic and plastic rarefaction waves ($R^E R^P$)

(d) Elastic shock wave (S^E)

(e) Plastic shock wave (R^P)

(f) Both elastic and plastic shock waves ($S^E S^P$)

Figure 1: The possible cases of Riemann solution structures in the left side.

4 Exact Riemann solver

Now we consider the constructing details of the exact Riemann solver. For the Riemann problem in Section 3, there are 6×6 possible cases in the Riemann solution with different wave structures. The left six cases are shown in Fig.1.

4.1 The solving process

From Section 3, we can find that all variables can be formulated in terms of the density. So we define equations

$$\begin{cases} f_u(\rho_L^*, \rho_R^*, \mathbf{Q}_L, \mathbf{Q}_R) = u_L^*(\rho_L^*, \mathbf{Q}_L) - u_R^*(\rho_R^*, \mathbf{Q}_R), \\ f_\sigma(\rho_L^*, \rho_R^*, \mathbf{Q}_L, \mathbf{Q}_R) = \sigma_L^*(\rho_L^*, \mathbf{Q}_L) - \sigma_R^*(\rho_R^*, \mathbf{Q}_R). \end{cases} \tag{4.1}$$

By using the relations across the contact wave in Section 3.1.3 and Section 3.2.2, we can get

$$\begin{cases} f_u(\rho_L^*, \rho_R^*, \mathbf{Q}_L, \mathbf{Q}_R) = u_L^*(\rho_L^*, \mathbf{Q}_L) - u_R^*(\rho_R^*, \mathbf{Q}_R) = 0, \\ f_\sigma(\rho_L^*, \rho_R^*, \mathbf{Q}_L, \mathbf{Q}_R) = \sigma_L^*(\rho_L^*, \mathbf{Q}_L) - \sigma_R^*(\rho_R^*, \mathbf{Q}_R) = 0. \end{cases} \tag{4.2}$$

Obviously, this system is uniquely solvable, but we can not get the analytical solution of (4.2). We have to use an iteration procedure to solve (4.2) and the solving process is shown in Fig.2. The details are introduced in the following.

Initial:

The initial densities are given as

$$\rho_{L(1)}^* = \frac{\rho_L + \rho_R}{2} \quad \rho_{R(1)}^* = \frac{\rho_L + \rho_R}{2}. \tag{4.3}$$

Iteration begin:

Step 1 Determining the case of the wave structure:

Given $\rho_{L(k)}^*$ and $\rho_{R(k)}^*$ in the k-th iteration step, we can use the method introduced in Section 4.2 to determine the case of wave structure of this Riemann problem. In the procedure for solving the Riemann problem, the subscript (k) means the variable in the k-th iteration step.

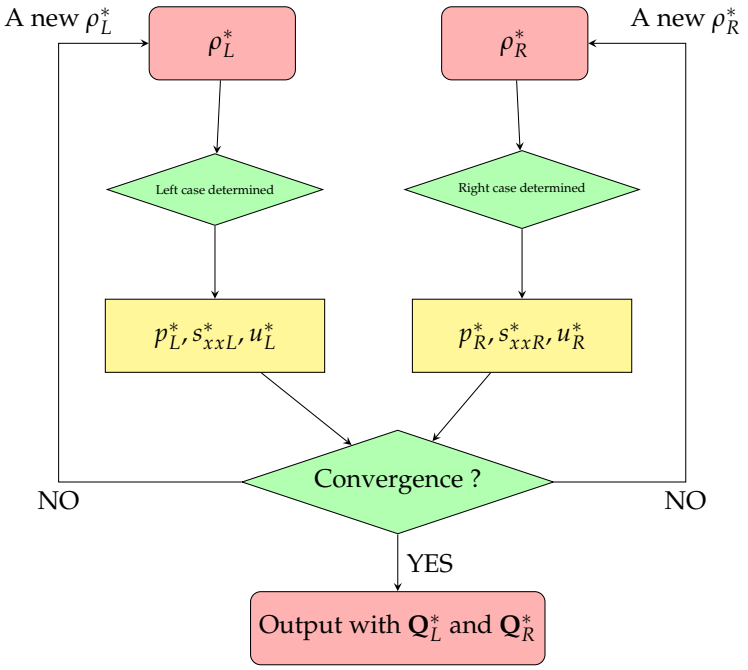

Figure 2: A flow chat of the Newton iteration process.

Step 2 Evaluating $f_{u(k)}$ and $f_{\sigma(k)}$:

After determining the structure case, we need to solve Cauchy stresses and velocities in regions $\mathbf{Q}_L^*$ and $\mathbf{Q}_R^*$, those are given in Section 4.4.

Step 3 Evaluating the derivatives of $f_{u(k)}$ and $f_{\sigma(k)}$.

The derivatives of $f_{u(k)}$ and $f_{\sigma(k)}$ are given as

$$\frac{\partial f_{u(k)}}{\partial \rho_{L(R)}^*} = \frac{f_{u(k)} - f_{u(k-1)}}{\rho_{L(R)(k)}^* - \rho_{L(R)(k-1)}}, \quad \frac{\partial f_{\sigma(k)}}{\partial \rho_{L(R)}^*} = \frac{f_{\sigma(k)} - f_{\sigma(k-1)}}{\rho_{L(R)(k)}^* - \rho_{L(R)(k-1)}}. \tag{4.4}$$

At the first step, we use a simple numerical difference method

$$\frac{\partial f_{u(1)}}{\partial \rho_{L(R)}^*} = \frac{f_u(\rho_{L(R)}^* + \Delta\rho) - f_u(\rho_{L(R)}^*)}{\Delta\rho_{L(R)}}, \quad \frac{\partial f_{u(1)}}{\partial \rho_{L(R)}^*} = \frac{f_u(\rho_{L(R)}^* + \Delta\rho) - f_u(\rho_{L(R)}^*)}{\Delta\rho_{L(R)}}, \tag{4.5}$$

where $\Delta\rho$ is a small quantity, we define it as

$$\Delta\rho = \frac{\rho_{L(R)(1)}^*}{100}. \tag{4.6}$$

Step 4 Evaluating $\rho_{L(k+1)}^*$ and $\rho_{R(k+1)}^*$:

$$\begin{bmatrix} \rho_{L(k+1)}^* \\ \rho_{R(k+1)}^* \end{bmatrix} = \begin{bmatrix} \rho_{L(k)}^* \\ \rho_{R(k)}^* \end{bmatrix} - \begin{bmatrix} \frac{\partial f_{u(k)}}{\partial \rho_L^*} & \frac{\partial f_{u(k)}}{\partial \rho_R^*} \\ \frac{\partial f_{\sigma(k)}}{\partial \rho_L^*} & \frac{\partial f_{\sigma(k)}}{\partial \rho_R^*} \end{bmatrix}^{-1} \begin{bmatrix} f_{u(k)} \\ f_{\sigma(k)} \end{bmatrix} \tag{4.7}$$

Step 5 Convergence test:

The iteration is convergent if

$$\text{CHA} \leq \text{TOL}, \tag{4.8}$$

Table 4.1: The condition of cases classification.

$\hat{\rho^*} < \rho$	$\hat{s}_{xx} < \frac{2}{3}Y_0$	$s_{xx} = \frac{2}{3}Y_0$ and $\hat{s}_{xx} \geq \frac{2}{3}Y_0$	other
	case a: R^E	case b: R^P	case c: $R^E R^P$
$\hat{\rho^*} > \rho$	$\hat{s}_{xx} > -\frac{2}{3}Y_0$	$s_{xx} = -\frac{2}{3}Y_0$ and $\hat{s}_{xx} \leq -\frac{2}{3}Y_0$	other
	case d: S^E	case e: S^P	case f: $S^E S^P$

where

$$\mathrm{CHA} = \max\left[\frac{|\rho^*_{L(k+1)} - \rho^*_{L,(k)}|}{\frac{1}{2}|\rho^*_{L(k+1)} + \rho^*_{L(k)}|}, \frac{|\rho^*_{R(k+1)} - \rho^*_{R,(k)}|}{\frac{1}{2}|\rho^*_{R(k+1)} + \rho^*_{R(k)}|}, |f_u|, |f_\sigma|\right], \tag{4.9}$$

$$\mathrm{TOL} = 10^{-4}.$$

If not, go to Step 1 and continue the iteration procedure until convergent. Numerical examples show, after 2-4 iterations, the condition (4.8) is satisfied.

Iteration end

4.2 Determining the case of structures

Given the value of density $\rho^*_{L(R)}$, we can distinguish the non-linear wave is a shock or rarefaction wave. This is done easily by comparing $\rho^*_{L(R)}$ with $\rho_{L(R)}$, the subscript $_{L(R)}$ means in the left(right) side of the contact wave.

$$\begin{cases} \text{a rarefaction wave:} & \text{if } \rho_{L(R)} > \rho^*_{L(R)}, \\ \text{a shock wave:} & \text{if } \rho_{L(R)} < \rho^*_{L(R)}. \end{cases} \tag{4.10}$$

Thanks to (3.13), the deviatoric stress can be evaluated as

$$\hat{s}_{xxL(R)} = -\frac{4}{3}\mu \ln\left(\frac{\rho^*_{L(R)}}{\rho_{L(R)}}\right) + s_{xxL(R)}. \tag{4.11}$$

According to the values of initial and evaluated deviatoric stresses in (4.11) in one side of the contact wave, the non-linear wave in this side may be:

$$\begin{cases} \text{an elastic rarefaction} & \text{if } \hat{s}_{xxL(R)} < \frac{2}{3}Y^0, \\ \text{a plastic rarefaction} & \text{if } s_{xxL(R)} = \frac{2}{3}Y^0 \text{ and } \hat{s}_{xxL(R)} \geq \frac{2}{3}Y_0, \\ \text{an elastic rarefaction and a following plastic rarefaction} & \text{if } s_{xxL(R)} < \frac{2}{3}Y_0 \text{ and } \hat{s}_{xxL(R)} \geq \frac{2}{3}Y_0, \\ \text{an elastic shock} & \text{if } \hat{s}_{xxL(R)} > -\frac{2}{3}Y_0, \\ \text{a plastic shock} & \text{if } s_{xxL(R)} = -\frac{2}{3}Y_0 \text{ and } \hat{s}_{xxL(R)} \leq -\frac{2}{3}Y_0, \\ \text{an elastic shock and a following plastic shock} & \text{if } s_{xxL(R)} > -\frac{2}{3}Y_0 \text{ and } \hat{s}_{xxL(R)} \leq -\frac{2}{3}Y_0. \end{cases} \tag{4.12}$$

Combining (4.10) and (4.12), we can find, in any side of the wave structure of this Riemann problem, there are six cases showed in Table 4.1, where capital letters "S" and "R" mean the shock and rarefaction wave, respectively; superscript letters "E" and "P" indicate the elastic or plastic state of a wave, respectively. Otherwise, the subscript L or R are omitted for simplification.

4.3 Evaluating states in middle regions ($\tilde{\mathbf{Q}}_L$ and $\tilde{\mathbf{Q}}_R$)

Cases (R^E, R^P, S^E and S^P)

For cases (R^E, R^P, S^E and S^P) in Fig.1, the material is totally yielding or totally not yielding, there is no midlle state $\tilde{\mathbf{Q}}_{L(R)}$. For expression convenience, we let

$$(\tilde{\rho}_{L(R)}, \tilde{u}_{L(R)}, \tilde{p}_{L(R)}, \tilde{s}_{xx}) = (\rho_{L(R)}, u_{L(R)}, p_{L(R)}, s_{xxL(R)}), \tag{4.13}$$

Case ($R^E R^P$)

Using the methods introduced in the Section (3.1.4), we can easily deduce the formulation of all unknown variables after the rarefaction wave. Here we do not show the details of deduction.

For the case ($R^E R^P$), after the elastic rarefaction wave, the deviatoric stress achieves the elastic limit. Thanks to (4.10) and (4.12), one can easily deduce that

$$\tilde{s}_{xxL(R)} = \frac{2}{3}Y_0.$$

By using (3.13), the density in $\tilde{\mathbf{Q}}_{L(R)}$ is given as

$$\tilde{\rho}_{L(R)} = \rho_{L(R)} \exp\left(-\frac{Y_0}{2\mu} + \frac{3s_{xxL(R)}}{4\mu}\right).$$

From (3.35) and (3.41), for the case ($R^E R^P$), the pressure is rearranged as

$$\tilde{p}_{L(R)} = p_{L(R)} e^{\frac{\lambda}{\rho_{L(R)}} - \frac{\lambda}{\tilde{\rho}_{L(R)}}} + e^{-\frac{\lambda}{\tilde{\rho}_{L(R)}}} \int_{\rho_{L(R)}}^{\tilde{\rho}_{L(R)}} f_2(x) e^{\frac{\lambda}{x}} dx, \tag{4.14}$$

where

$$\lambda = \rho_0 \Gamma_0 \quad f_2(\rho) = a_0^2 \frac{\partial f}{\partial \eta} - \lambda \frac{s_{xx}(\rho)}{\rho^2}, \; s_{xx}(\rho) = -\frac{4}{3}\mu \ln\left(\frac{\rho}{\rho_{L(R)}}\right) + s_{xxL(R)}.$$

Thanks to (3.36) and (3.42), for the rarefaction wave case ($R^E R^P$), the velocity is given as

$$\tilde{u}_{L(R)} = \begin{cases} u_L - \displaystyle\int_{\rho_L}^{\tilde{\rho}_{L(R)}} \frac{c_e(x)}{x} dx & \text{for the left-going rarefaction wave,} \\ u_R + \displaystyle\int_{\rho_R}^{\tilde{\rho}_{L(R)}} \frac{c_e(x)}{x} dx & \text{for the right-going rarefaction wave,} \end{cases} \tag{4.15}$$

where the sonic speed

$$c_e(\rho) = \sqrt{a_0^2 \frac{\partial f}{\partial \eta} + \frac{p(\rho)}{\rho^2}\rho_0\Gamma_0 - \frac{\rho_0}{\rho^2}\Gamma_0 s_{xx}(\rho) + \frac{4}{3}\frac{\mu}{\rho}}.$$

Remark 1: In (4.14) and (4.15), there are two integral terms. Obviously, because of the complexity of the EOS, we can not get the exact integral values. We have to use the numerical methods to approximate the two integral terms with high order of accuracy. The approximation methods are introduced in the Appendix A.

Case ($S^E S^P$)

Using the methods introduced in the Section (3.1.5), we can easily deduce the formulation of all unknown variables in $\tilde{\mathbf{Q}}_{L(R)}$. In order to shorten the length of our paper, we do not show the details of the deduction.

For the case ($S^E S^P$), after the elastic shock wave, the deviatoric stress achieves the elastic limit. So, by using (4.10) and (4.12), one can easily deduce that

$$\tilde{s}_{xxL(R)} = -\frac{2}{3}Y_0.$$

From (3.13), after the elastic shock wave, the density in $\tilde{\mathbf{Q}}_{L(R)}$ is given as

$$\tilde{\rho}_{L(R)} = \rho_{L(R)} \exp\left(\frac{Y_0}{2\mu} + \frac{3s_{xxL(R)}}{4\mu}\right).$$

By using (3.52), the pressure can be solved as

$$\tilde{p}_{L(R)} = \frac{2t(c_1 f(\tilde{\rho}_{L(R)}/\rho_0) + e_{L(R)}) - (\sigma_{L(R)} + \tilde{s}_{xxL(R)})}{2tc_0 - 1}, \tag{4.16}$$

where $c_0 = \frac{1}{\rho_0\Gamma_0}$, $c_1 = \frac{a_0^2}{\Gamma_0}$ and $t = \frac{\rho_{L(R)}\tilde{\rho}_{L(R)}}{\tilde{\rho}_{L(R)} - \rho_{L(R)}}$.

Thanks to (3.55), the velocity can be written as

$$\begin{cases} \tilde{u}_L = u_L - \sqrt{\frac{\sigma_L - \tilde{\sigma}_L}{t}}, \\ \tilde{u}_R = u_R + \sqrt{\frac{\sigma_R - \tilde{\sigma}_R}{t}}, \end{cases} \tag{4.17}$$

where

$$\tilde{\sigma}_{L(R)} = -\tilde{p}_{L(R)} + \tilde{s}_{xxL(R)}. \tag{4.18}$$

4.4 Evaluating states in regions $\mathbf{Q}_L^*$ and $\mathbf{Q}_R^*$

Rarefaction wave cases (R^E, R^P and $R^E R^P$)

For the three rarefaction wave cases, thanks to (3.13) and (3.57), s_{xx} in $\mathbf{Q}_L^*$ and $\mathbf{Q}_R^*$ are

$$s^*_{xxL(R)} = \begin{cases} -\frac{4}{3}\mu \ln\left(\frac{\rho^*_{L(R)}}{\tilde{\rho}_{L(R)}}\right) + s_{xxL(R)} & \text{for case } (R^E), \\ \frac{2}{3}Y_0 & \text{for cases } (R^P \text{ and } R^E R^P). \end{cases}$$

From (4.14), the pressure in the star region is

$$p^*_{L(R)} = \tilde{p}_{L(R)} e^{\frac{\lambda}{\rho_{L(R)}} - \frac{\lambda}{\rho}} + e^{-\frac{\lambda}{\rho^*_{L(R)}}} \int_{\tilde{\rho}_{L(R)}}^{\rho^*_{L(R)}} f_2(x) e^{\frac{\lambda}{x}} dx, \tag{4.19}$$

where

$$\lambda = \rho_0\Gamma_0 \quad f_2(\rho) = a_0^2 \frac{\partial f}{\partial \eta} - \lambda \frac{s_{xx}(\rho)}{\rho^2}, \; s_{xx}(\rho) = -\frac{4}{3}\mu \ln\left(\frac{\rho}{\rho_{L(R)}}\right) + s_{xxL(R)}.$$

By Equations (3.36) and (3.42) the velocity in regions $\mathbf{Q}_L^*$ and $\mathbf{Q}_R^*$ can be written as

$$u^*_{L(R)} = \begin{cases} \tilde{u}_L - \int_{\rho_L}^{\rho^*_{L(R)}} \frac{c(x)}{x} dx, \\ \tilde{u}_R + \int_{\rho_R}^{\rho^*_{L(R)}} \frac{c(x)}{x} dx, \end{cases} \tag{4.20}$$

where

$$c(\rho) = \begin{cases} \sqrt{a_0^2 \frac{\partial f}{\partial \eta} + \frac{p(\rho)}{\rho^2}\rho_0\Gamma_0 - \frac{\rho_0}{\rho^2}\Gamma_0 s_{xx}(\rho) + \frac{4}{3}\frac{\mu}{\rho}} & \text{for case } (R^E), \\ \sqrt{a_0^2 \frac{\partial f}{\partial \eta} + \frac{p(\rho)}{\rho^2}\rho_0\Gamma_0 - \frac{\rho_0}{\rho^2}\Gamma_0 s_{xx}(\rho)} & \text{for cases } (R^P \text{ and } R^E R^P). \end{cases}$$

Remark 2: Just like **Remark 1**, we have to use numerical integral methods introduced in the Appendix A to evaluate the integral terms in (4.19) and (4.20).

Shock wave cases (S^E, S^P and $S^E S^P$)

For shock waves cases, the deviatoric stresses in $\mathbf{Q}_L^*$ and $\mathbf{Q}_R^*$ are given as

$$s_{xx}(\rho) = \begin{cases} -\frac{4}{3}\mu \ln\left(\frac{\rho}{\tilde{\rho}_{L(R)}}\right) + \tilde{s}_{xxL(R)}, & \text{case } (S^E), \\ -\frac{2}{3}Y_0, & \text{cases } (S^P \text{ and } S^E S^P). \end{cases} \tag{4.21}$$

Figure 3: Half Riemann problem with a given left velocity or Cauchy stress..

(3.52) gives direct expressions for the By the equation of (3.52), the pressure is given as

$$p^*_{L(R)} = \frac{2t\left(c_1 f(\rho^*_{L(R)}/\rho_0) + \tilde{e}_{L(R)}\right) - \left(\tilde{\sigma}_{L(R)} + s_{xx}(\rho^*_{L(R)})\right)}{2tc_0 - 1}, \tag{4.22}$$

where $c_0 = \frac{1}{\rho_0\Gamma_0}$, $c_1 = \frac{a_0^2}{\Gamma_0}$ and $t = \frac{\rho^*_{L(R)}\tilde{\rho}_{L(R)}}{\rho^*_{L(R)} - \tilde{\rho}_{L(R)}}$.

Thanks to (3.55), the velocities in $\mathbf{Q}^*_L$ and $\mathbf{Q}^*_R$ are

$$u^*_{L(R)} = \begin{cases} \tilde{u}_L - \sqrt{\dfrac{\tilde{\sigma}_L - \sigma^*_{L(R)}}{t}} & \text{for the left-going shock wave,} \\ \tilde{u}_R + \sqrt{\dfrac{\tilde{\sigma}_R - \sigma^*_{L(R)}}{t}} & \text{for the right-going shock wave,} \end{cases} \tag{4.23}$$

where $\sigma^*_{L(R)} = -p^*_{L(R)} + s^*_{xxL(R)}$.

5 Half Riemann problem and its solver

Sometimes we need to analyse a half Riemann problem with a given velocity or Cauchy stress. Shown in Fig.3, in these cases, we only need to solve states in one side. There are six possible cases just like them in Section 3. Here we will use the example shown in Fig.3 to show how to solve the half Riemann problem.

As we know the velocity u^* or the Cauchy stress σ^* on the left, there is only one equation need to be solved:

$$f(\rho^*, \mathbf{Q}_R) = u(\rho^*, \mathbf{Q}_R) - u^* = 0, \tag{5.1}$$

or

$$f(\rho^*, \mathbf{Q}_R) = \sigma(\rho^*, \mathbf{Q}_R) - \sigma^* = 0. \tag{5.2}$$

Similar to the process in Section (4.1), we have to use an iteration procedure to solve (5.1) or (5.2) and the solving process is list in the following.

Initial:

The initial density is given as

$$\rho^*_{(1)} = \rho_R. \tag{5.3}$$

Iteration begin:

Step 1 Determine the case of the wave structure:

Given the value of $\rho^*_{(k)}$ in the k-th iteration step, use the methods introduced in Section 4.2 to determine the case of wave structure of this Riemann problem. Here the subscript (k) means the variable in the k-th iteration step.

Step 2 Solve $f(\rho^*, \mathbf{Q}_R)$:

After determining the structure case, evaluate the velocity (or the Cauchy stress) in the region $\mathbf{Q}^*$ and the details are given in Section 4.4.

Step 3 Evaluate the derivative of $f(\rho^*, \mathbf{Q}_R)$:

The derivatives of f is given by

$$\frac{\partial f_{(k+1)}}{\partial \rho^*} = \frac{f_{(k+1)} - f_{(k)}}{\rho^*_{(k+1)} - \rho^*_{(k)}}, \tag{5.4}$$

At the first step, we use a simple numerical difference method

$$\frac{\partial f_{(1)}}{\partial \rho^*} = \frac{f(\rho^* + \Delta\rho) - f(\rho^*)}{\Delta\rho}, \tag{5.5}$$

where $\Delta\rho$ is a small quantity, here we set $\Delta\rho = \frac{\rho^*_{(1)}}{100}$.

Step 4 Evaluate $\rho^*_{(k+1)}$:

A new density can be updated by

$$\rho^*_{(k+1)} = \rho^*_{(k)} - f/\frac{\partial f_{(k)}}{\partial \rho}. \tag{5.6}$$

Step 5 Convergence test:

The iteration is convergent if

$$\text{CHA} \leq \text{TOL}, \tag{5.7}$$

where

$$\text{CHA} = \max\left[\frac{|\rho^*_{(k+1)} - \rho^*_{(k)}|}{\frac{1}{2}|\rho^*_{(k+1)} + \rho^*_{(k)}|}, |f|\right], \quad \text{TOL} = 10^{-4}.$$

If not, go to Step 1 and continue the iteration procedure until convergent. Numerical examples show, after 2-4 iterations, the condition (5.7) is satisfied.

Iteration end.

6 Numerical tests

In this section, by choosing different initial conditions, we will solve different Riemann problems with several different wave structures in the solutions. In order to verify the correctness of our exact Riemann solver, we use a third-order numerical scheme for 1D elastic-plastic flows introduced in [5] to evaluate these Riemann problems and compare numerical results with our exact solution.

In the following tests, the materials are taken as aluminium and copper. The parameters for the EOS and constitutive model for aluminum and copper are $(\rho_0, a_0, \Gamma_0, s, \mu)_{\text{Al}} = (8930\text{kg/m}^3, 3940\text{m/s}, 2, 1.49, 2.76, 2.76\times 10^{10}\text{Pa})$ and $(\rho_0, a_0, \Gamma_0, s, \mu)_{\text{copper}} = (2785\text{kg/m}^3, 5328\text{m/s}, 2, 1.338, 4.5\times 10^{10}\text{Pa})$, respectively. The yielding strengths of the two materials are $Y_{0,\text{Al}} = 3\times 10^8\text{Pa}$ and $Y_{0,\text{Copper}} = 9\times 10^7\text{Pa}$, respectively. The computational domain is set to be $[0, 1m]$ with 800 cell points and the intial interface is located at $0.5m$, the terminal time is $t = 5\times 10^{-5}s$. Otherwise, in the initial condition, "L" and "R" mean $x < 0.5m$ and $x > 0.5m$, respectively.

6.1 Test 1

In this case, the material is yielding at both sides, so the solution structure has three wave with two plastic shock waves and one contact. The initial condition is

$$\begin{cases} \text{L: Al}, \quad \rho = 2785\text{kg/m}^3, \quad u = 20\text{m/s}, \quad p = 1.0\text{Pa}, \quad s_{xx} = -2.0\times 10^8\text{Pa}, \\ \text{R: Al}, \quad \rho = 2785\text{kg/m}^3, \quad u = 0\text{m/s}, \quad p = 1.0\text{Pa}, \quad s_{xx} = -2.0\times 10^8\text{Pa}, \end{cases} \tag{6.1}$$

It can be seen that the exact solution matches the numerical results very well in Fig.4.

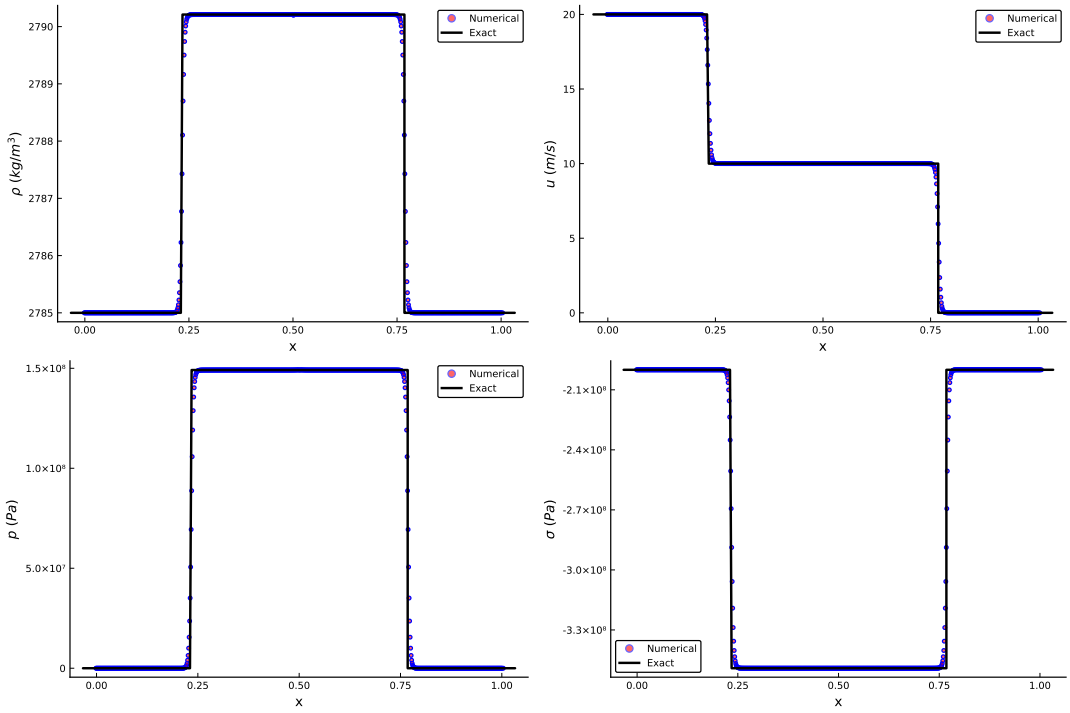

Figure 4: Comparison results for Test 1 with the structures of $S^P|S^P$.

6.2 Test 2

Here we consider a case with yielding process at both sides, so there are five waves in the wave structure of this Riemann problem. The initial condition is

$$\begin{cases} \text{L: Al}, \quad \rho = 2785\text{kg/m}^3, \quad u = 800\text{m/s}, \quad p = 1.0\text{Pa}, \quad s_{xx} = 0.0\text{Pa}, \\ \text{R: Al}, \quad \rho = 2785\text{kg/m}^3, \quad u = 0\text{m/s}, \quad p = 1.0\text{Pa}, \quad s_{xx} = 0.0\text{Pa}, \end{cases} \tag{6.2}$$

Shown in Fig.5, the exact solution matches the numerical results well generally, except the under-cooling effect performed in the numerical results, but it is not considered in the designing of the exact Riemann solver.

6.3 Test 3

In this example, we test the case with two elastic rarefaction waves. In the wave structure there is one elastic rarefaction wave on each side of the contace wave. The initial condition is given as

$$\begin{cases} \text{L: Al}, \quad \rho = 2785\text{kg/m}^3, \quad u = -2.0\text{m/s}, \quad p = 1.0^7\text{Pa}, \quad s_{xx} = 0.0\text{Pa}, \\ \text{R: Al}, \quad \rho = 2785\text{kg/m}^3, \quad u = 2.0\text{m/s}, \quad p = 1.0 \times 10^7\text{Pa}, \quad s_{xx} = 0.0\text{Pa}, \end{cases} \tag{6.3}$$

We can see that the results of the exact solution match the numerical results very well.

6.4 Test 4

In this test we test the example with both elastic and plastic rarefaction waves on both sides of contact wave. The initial condition is

$$\begin{cases} \text{L: Al}, \quad \rho = 2785\text{kg/m}^3, \quad u = -40\text{m/s}, \quad p = 1.0 \times 10^7\text{Pa}, \quad s_{xx} = 0.0\text{Pa}, \\ \text{R: Al}, \quad \rho = 2785\text{kg/m}^3, \quad u = 40\text{m/s}, \quad p = 1.0 \times 10^7\text{Pa}, \quad s_{xx} = 0.0\text{Pa}. \end{cases} \tag{6.4}$$

Results are shown in Fig.7, the results of the exact solver matches the numerical results very well.

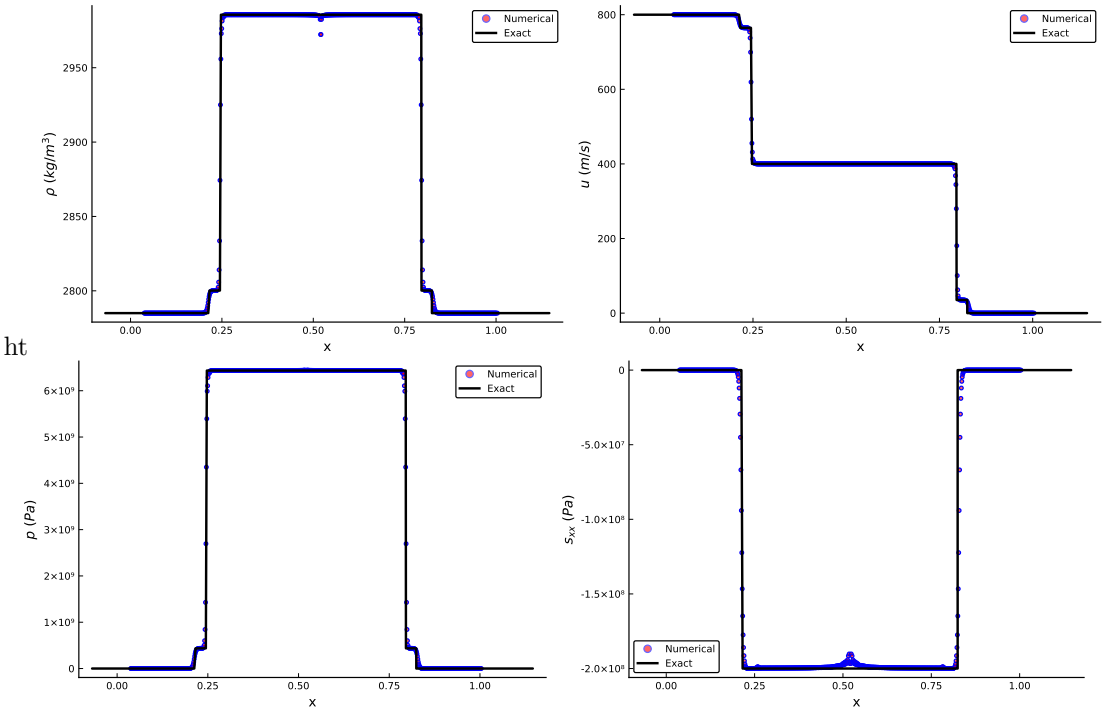

Figure 5: Comparison results for Test 2 with the structures of $S^E S^P | S^P S^E$.

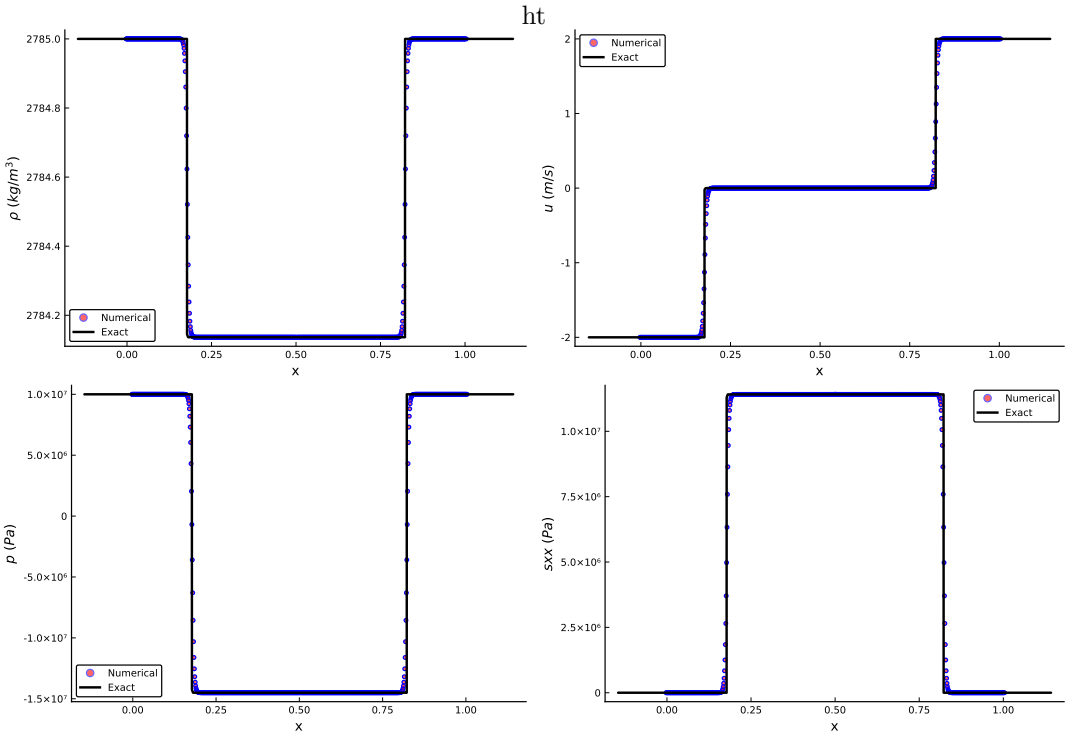

Figure 6: Comparison results for Test 3 with the wave structures of $R^E | R^E$.

ht

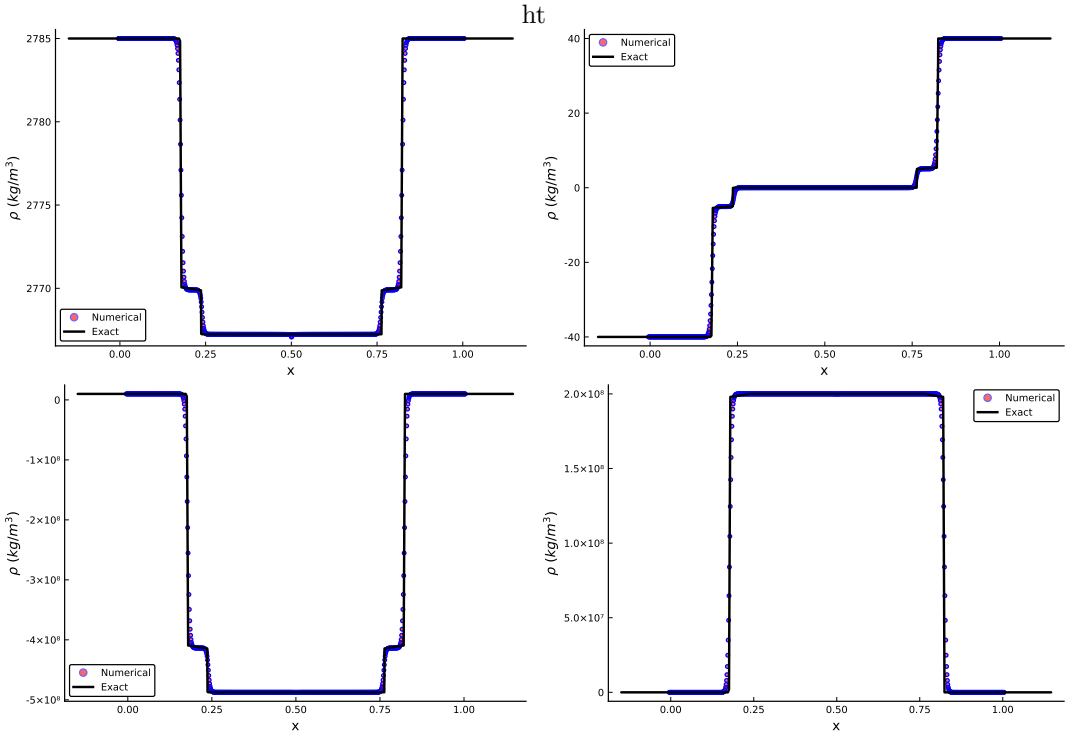

Figure 7: Comparison results for Test 4 with the wave structures of $R^E R^P | R^P R^E$.

6.5 Test 5

The initial condition of this Riemann problem is

$$\begin{cases} \text{L: Al}, \quad \rho = 2785\text{kg/m}^3, \quad u = -200\text{m/s}, \quad p = 1.0\text{Pa}, \quad s_{xx} = -2.0^8\text{Pa}, \\ \text{R: Al}, \quad \rho = 2785\text{kg/m}^3, \quad u = 0\text{m/s}, \quad p = 1.0\text{Pa}, \quad s_{xx} = -2.0^8\text{Pa}. \end{cases} \tag{6.5}$$

From the initial condition, at the beginning, the material is in the negative plastic state (i.e. $s_{xxL(R)} = -\frac{2}{3}Y^0$). If using the thought introduced by Gao and Liu, the material will be always in the negative plastic state. Exact solutions based on this thought are denoted by blue solid lines in Fig.8. Obviously, from Fig.8, one can find that the exact solutions denoted by blue solid lines are wrong because they do not match the numerical results very seriously. On the contrary, according to the analysis introduced in Section "Introduction", we can get the right exact solutions which match the numerical solutions very well in Fig.8 . This shows our analysis in Section "Introduction" is right.

6.6 Test 6

All the above five tests have symmetrical wave structures, here we will test an example with different structures on two sides: one plastic shock on the left side and both the elastic and plastic shocks on the right of one contact wave. The initial condition is given as

$$\begin{cases} \text{L: Al}, \quad \rho = 2785\text{kg/m}^3, \quad u = 40\text{m/s}, \quad p = 1.0 \times 10^8\text{Pa}, \quad s_{xx} = -2.0 \times 10^8\text{Pa}, \\ \text{R: Al}, \quad \rho = 2785\text{kg/m}^3, \quad u = -40\text{m/s}, \quad p = 1.0 \times 10^2\text{Pa}, \quad s_{xx} = 0.0\text{Pa}. \end{cases} \tag{6.6}$$

The solutions of this test are shown in Fig.9. From this figure, we can find the exact solutions match numerical solutions very well.

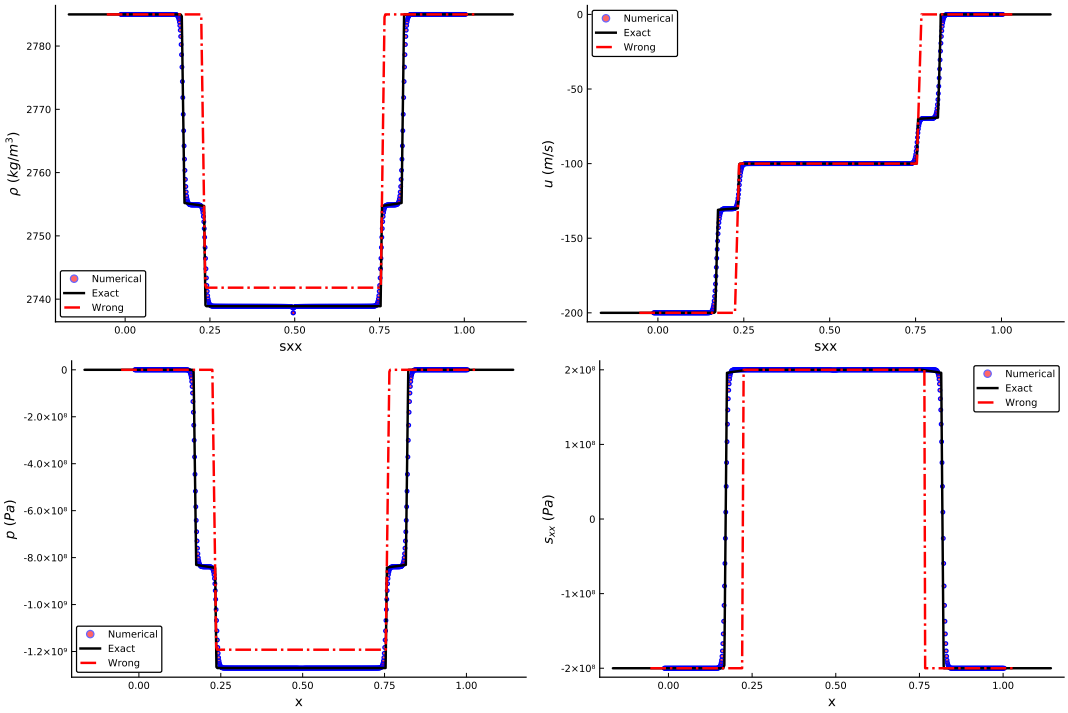

Figure 8: Comparison results for Test 5 with the structures of $R^E R^P | R^P R^E$.

6.7 Test 7

In this test, we consider an example with zero initial velocities on both sides, driving by the gradient of the pressure, there are rarefaction waves produced into the higher pressure side and shock waves generated into the lower pressure side. The initial condition is given as

$$\begin{cases} \text{L: Al}, \quad \rho = 2785\text{kg/m}^3, \quad u = 0.0\text{m/s}, \quad p = 1.0 \times 10^{10}\text{Pa}, \quad s_{xx} = 0.0\text{Pa}, \\ \text{R: Al}, \quad \rho = 2785\text{kg/m}^3, \quad u = 0.0\text{m/s}, \quad p = 1.0 \times 10^{2}\text{Pa}, \quad s_{xx} = 0.0\text{Pa}. \end{cases} \tag{6.7}$$

Shown in Fig.13, we can see there are two shocks in the right side and two rarefaction waves on the left side.

6.8 Test 8

Now we will consider two multi-material tests with different materials on both sides. In this test, on the left side, a lighter material of aluminum with a velocity impact to a heavier material of Copper. The initial condition is given as

$$\begin{cases} \text{L: Al}, \quad \rho = 2785\text{kg/m}^3, \quad u = 40\text{m/s}, \quad p = 0.1\text{Pa}, \quad s_{xx} = 0.0\text{Pa}, \\ \text{R: Copper}, \quad \rho = 8930\text{kg/m}^3, \quad u = 0.0\text{m/s}, \quad p = 0.1\text{Pa}, \quad s_{xx} = 0.0\text{Pa}. \end{cases} \tag{6.8}$$

Show in the Fig.11, there is a large jump of density at the material interface and both elastic shock and plastic shock exist in each side of the interface. Comparing to the numerical results of the scheme with MHLLCEP approximate solver, we can find that our exact Riemann solver can solve the Riemann problem with multi-materials very well.

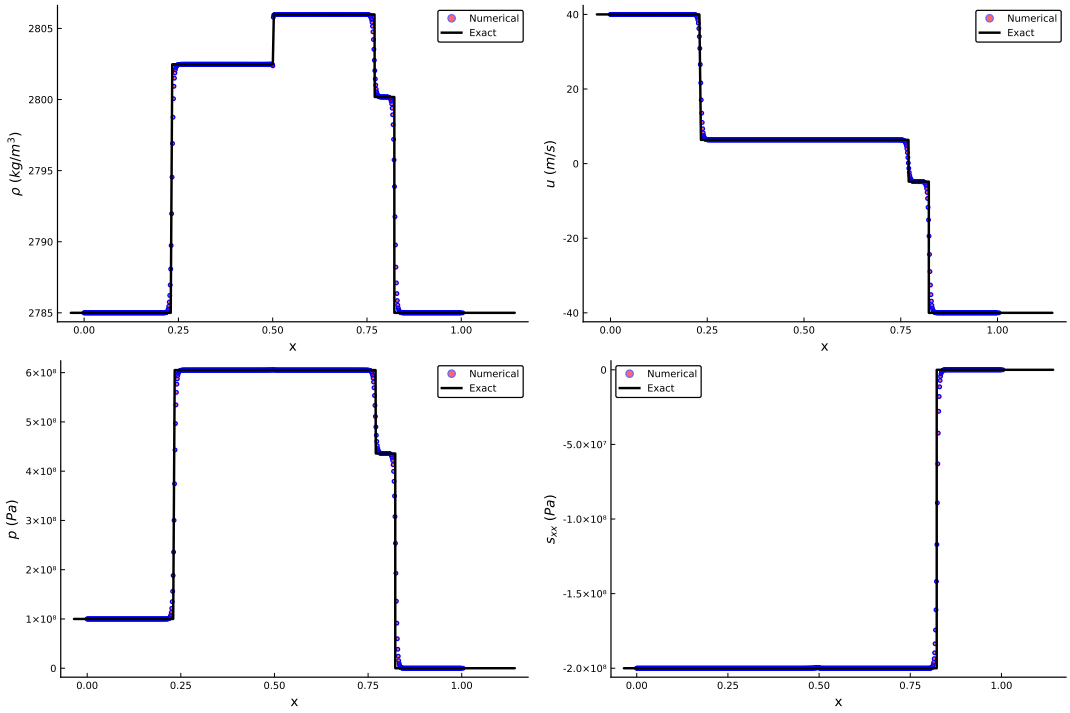

Figure 9: Comparison resutls for Test 6 with the structrures of $R^P|R^PR^E$.

6.9 Test 9

Here we test another multi-materials case, in this test the initial condition is given as

$$\begin{cases} \text{L: Copper}, \quad \rho = 8930\text{kg/m}^3, \quad u = 0.0\text{m/s}, \quad p = 1.0 \times 10^{10}\text{Pa}, \quad s_{xx} = 0.0\text{Pa}, \\ \text{R: Al}, \quad \rho = 2785\text{kg/m}^3, \quad u = 0\text{m/s}, \quad p = 10.0\text{Pa}, \quad s_{xx} = 0.0\text{Pa}. \end{cases} \tag{6.9}$$

Shown in Fig.12, there are two rarefaction waves on the left side and two shocks on the right side, there is the discontinuity of pressure on the interface, and the Cauchy stress is continuous, which satisfies the theoretical analysis.

6.10 Test 10

This test is a half Riemann problem with a given left velocity $u^* = -20\text{m/s}$, and the right initial condition is

$$\text{Copper}, \quad \rho = 8930\text{kg/m}^3, \quad u = 0.0\text{m/s}, \quad p = 0.1\text{Pa}, \quad s_{xx} = 0.0\text{Pa}. \tag{6.10}$$

In Fig.13, comparison results are given by the exact half Riemann solver and the numerical method. We can see that the exact solver can resolve both the elastic and plastic shock waves very well.

6.11 Test 11

The second half Riemann case is with a given left Cauchy stress $\sigma^* = 0\text{Pa}$, and the right initial condition is

$$\text{Copper}, \quad \rho = 8930\text{kg/m}^3, \quad u = 0.0\text{m/s}, \quad p = 1.0 \times 10^9\text{Pa}, \quad s_{xx} = 0.0\text{Pa}. \tag{6.11}$$

In Fig.14, we give the results computed by the exact Riemann solver and the numerical simulation. From this figure one can see, the exact solver can resolve the elastic and plastic rarefaction waves well.

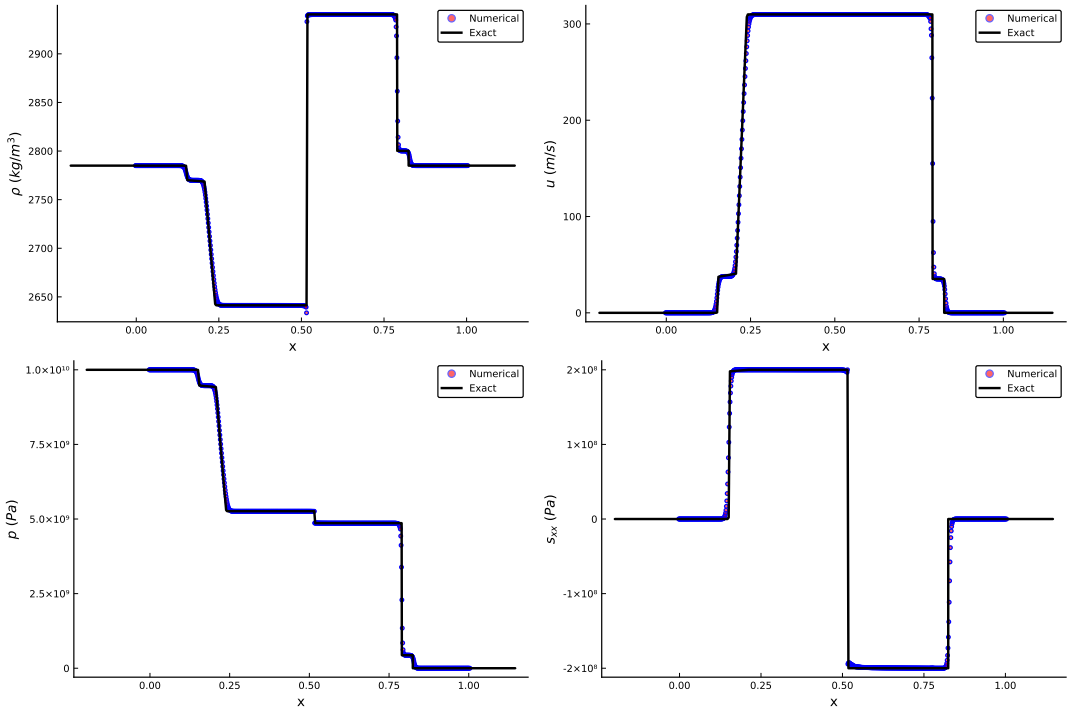

Figure 10: Comparison resutls for Test 7 with the structrures of $R^E R^P | S^P S^E$.

7 Results

In this paper, we give a detailed analysis of the Riemann problem for one-dimensional multi-material elastic-plastic flows with the Mie-Grüneisen EOS, hypo-elastic constitutive model and the von Mises' yielding condition. Some useful results are found through the analysing:

1. The sonic speed periods a significant jump when the material is yielding.
2. the plastic wave is always faster than the elastic wave for the reason of the sonic speed jump.
3. There are only thirty-six possible cases of the structrues in the Riemann problem.
4. All the variables after the wave can be written as functions of the density theoretically.
5. if the initial material is in the negative plastic state, after being expanded, the material may be into the elastic state or the positive plastic state.
6. if the initial material is in the positive plastic state, after being compressed, the material may be into the elastic state or the negative plastic state.

Then, based on the above analysis, we have constructed exact Riemann solvers for both the Riemann problem and the half Riemann problem, separately. Tested by a large number of examples, the exact Riemann solver is reasonable and its solutions are matching well with the numerical results for both single material problems and multi-material Riemann problems.

Acknowledgement

This work was supported by NSFC(Grant No. 11672047) and Science Challenge Project (Grant No. TZ2016002).

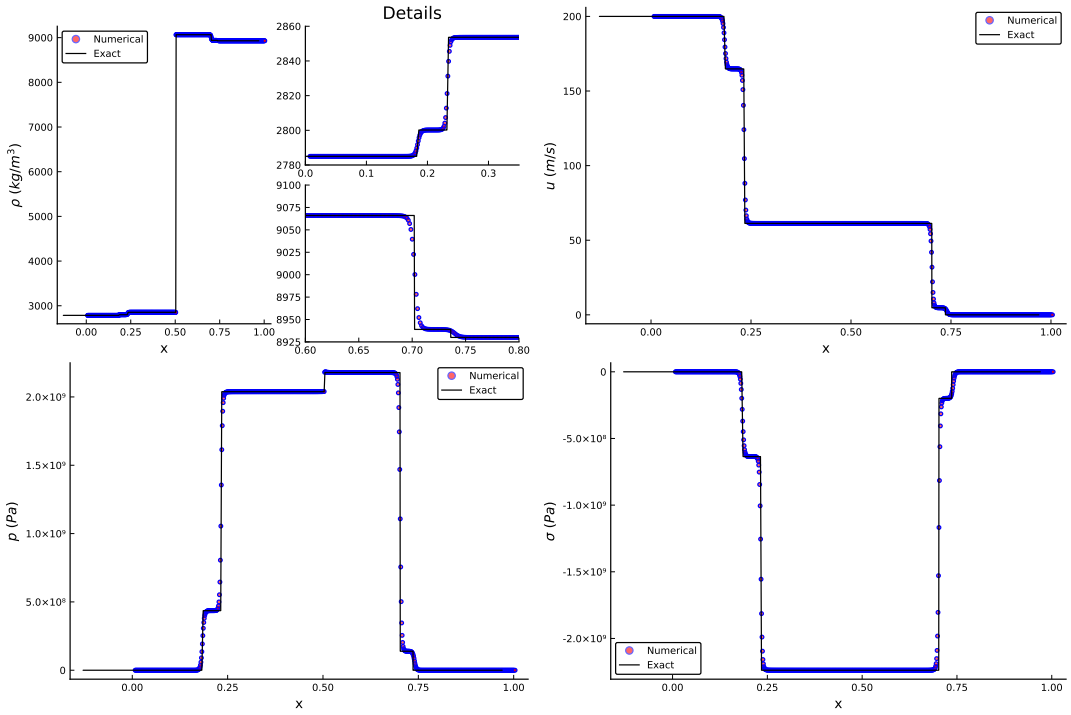

Figure 11: Comparison results for Test 8 with structures of $R^E R^P | R^P R^E$.

References

[1] M. L. Wilkins, Calculation of elastic-plastic flow, Tech. rep., California Univ Livermore Radiation Lab (1963).

[2] S. L. Gavrilyuk, N. Favrie, R. Saurel, Modelling wave dynamics of compressible elastic materials, Journal of computational physics 227 (5) (2008) 2941–2969.

[3] J.-B. Cheng, E. F. Toro, S. Jiang, M. Yu, W. Tang, A high-order cell-centered Lagrangian scheme for one-dimensional elastic–plastic problems, Computers & Fluids 122 (2015) 136–152.

[4] J. Cheng, Harten-Lax-van Leer-contact (HLLC) approximation Riemann solver with elastic waves for one-dimensional elastic-plastic problems, Applied Mathematics and Mechanics 37 (11) (2016) 1517–1538.

[5] L. Liu, J.-b. Cheng, A multi-material HLLC Riemann solver with both elastic and plastic waves for 1D elastic-plastic flows, https://www.researchgate.net/publication/332709456_A_multi-material_HLLC_Riemann_solver_with_both_elastic_and_plastic_waves_for_1D_elastic-plastic_flows, (preprint).

[6] X. Garaizar, Solution of a Riemann problem for elasticity, Journal of elasticity 26 (1) (1991) 43–63.

[7] G. H. Miller, An iterative riemann solver for systems of hyperbolic conservation laws, with application to hyperelastic solid mechanics, Journal of Computational Physics 193 (1) (2004) 198–225.

[8] S. Gao, T. Liu, 1d exact elastic-perfectly plastic solid Riemann solver and its multi-material application, Advances in Applied Mathematics and Mechanics 9 (3) (2017) 621–650.

[9] S. Gao, T. Liu, C. Yao, A complete list of exact solutions for one-dimensional elastic-perfectly plastic solid riemann problem without vacuum, Communications in Nonlinear Science and Numerical Simulation 63 (2018) 205–227.

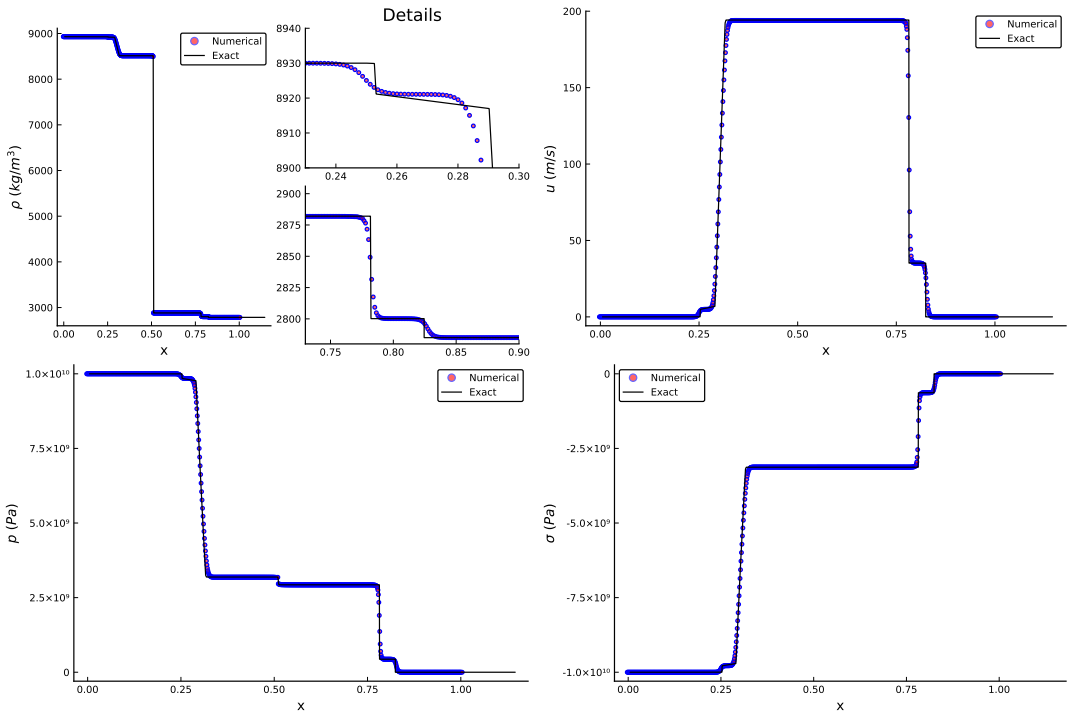

Figure 12: Comparison results for Test 9 with the structures of $R^E R^P | S^E S^P$.

[10] P.-H. Maire, R. Abgrall, J. Breil, R. LoubèRe, B. Rebourcet, A nominally second-order cell-centered Lagrangian scheme for simulating elastic–plastic flows on two-dimensional unstructured grids, Journal of Computational Physics 235 (2013) 626–665.

A Numerical intergration for the rarefaction wave

There are two integrations in functions $p(\rho)$ and $u(\rho)$ in the rarefaction wave, for example, in the equations (4.14) and (4.15). In this paper, we use a seventh-order (with 4 integrating points) Gaussian quadrature to make numerical integrations. For a function $g(x)$, the Gaussian integration from -1 to 1 is given as

$$\int_{-1}^{1} g(x)dx \approx \sum_{i=1}^{n} \omega_i g(x_i),$$

ω_i is the weight, and x_i is the integrating point. For seventh-order, integrating points and corresponding weights are

$$x_1,\ x_2 = \pm\sqrt{\frac{3}{7} - \frac{2}{7}\sqrt{\frac{6}{5}}} \quad \left(\omega_1,\ \omega_2 = \frac{18+\sqrt{30}}{36}\right),$$

$$x_3,\ x_4 = \pm\sqrt{\frac{3}{7} + \frac{2}{7}\sqrt{\frac{6}{5}}} \quad \left(\omega_3,\ \omega_4 = \frac{18-\sqrt{30}}{36}\right).$$

Then for a function over $[\rho_0, \rho]$, this change of interval can be done in the following way:

$$\int_{\rho_0}^{\rho} g(x)dx = \frac{\rho-\rho_0}{2}\int_{-1}^{1} g\left(\frac{\rho-\rho_0}{2}x + \frac{\rho_0+\rho}{2}\right)dx.$$

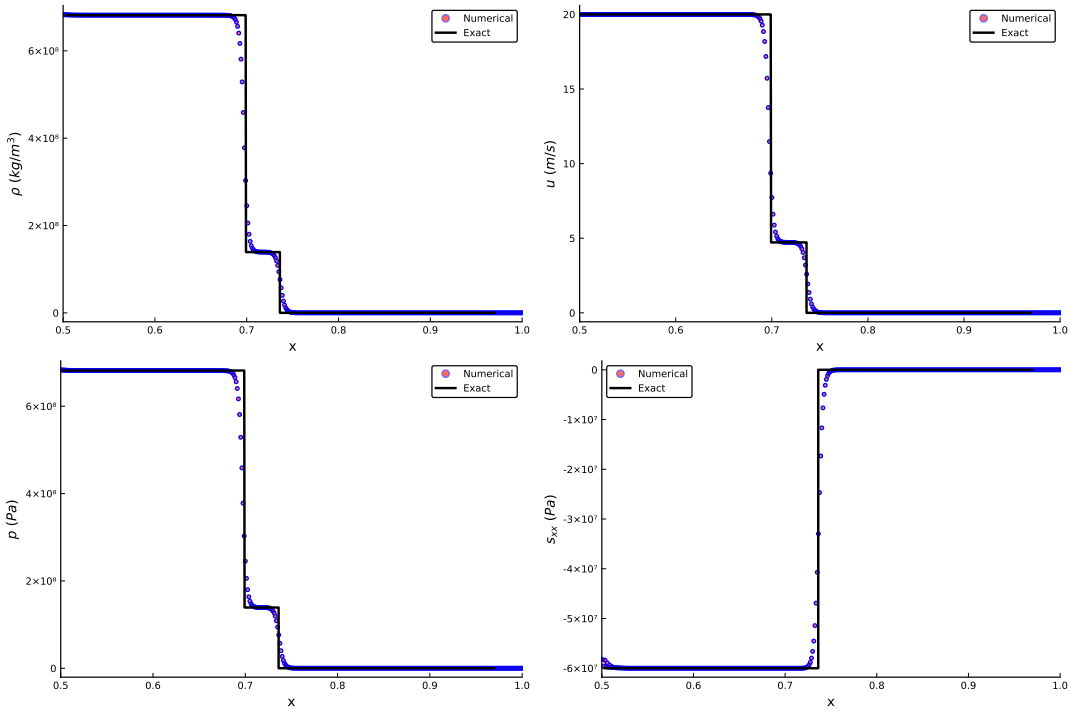

Figure 13: Comparison results for Test 10 with the structures of $S^E S^P$.

At last, we can get

$$\int_{\rho_0}^{\rho} g(x)dx \approx \frac{\rho-\rho_0}{2}\sum_{i=1}^{n}\omega_i g\left(\frac{\rho-\rho_0}{2}x_i+\frac{\rho_0+\rho}{2}\right). \tag{A.1}$$

Integrating of $p(\rho)$
Taking Equation (4.14) as an example,

$$p(\rho) \approx p_{L(R)} e^{\frac{\lambda}{\rho_{L(R)}}-\frac{\lambda}{\rho}} + e^{-\frac{\lambda}{\rho}}\mathrm{Intg}_1, \tag{A.2}$$

where

$$\mathrm{Intg}_1 = \frac{\rho-\rho_{L(R)}}{2}\sum_{n=1}^{4}\omega_i f_2(\rho_i) e^{\lambda/\rho_i},$$

and $\rho_i = \frac{\rho-\rho_{L(R)}}{2}x_i + \frac{\rho_{L(R)}+\rho}{2}$.
Obviously, we can use (A.2) to evaluate all the values of $p(\rho_i)$ on all Gaussian quadrature points.
Integrating of $u(\rho)$
Taking Equation (4.15) as an example, if the wave is on the left side

$$u(\rho) = u_L - \int_{\rho_L}^{\rho}\frac{c_e(x)}{x}dx.$$

The numerical intergration of $u(\rho)$ is given as

$$u(\rho) \approx u_L - \mathrm{Intg}_2 \tag{A.3}$$

where

$$\mathrm{Intg}_2 = \frac{\rho-\rho_{L(R)}}{2}\sum_{n=1}^{4}\omega_i\frac{c_e(\rho_i)}{\rho_i},$$

Different from (A.2), the sonic speed $c_e(\rho_i)$ is dependent on $p(\rho_i)$:

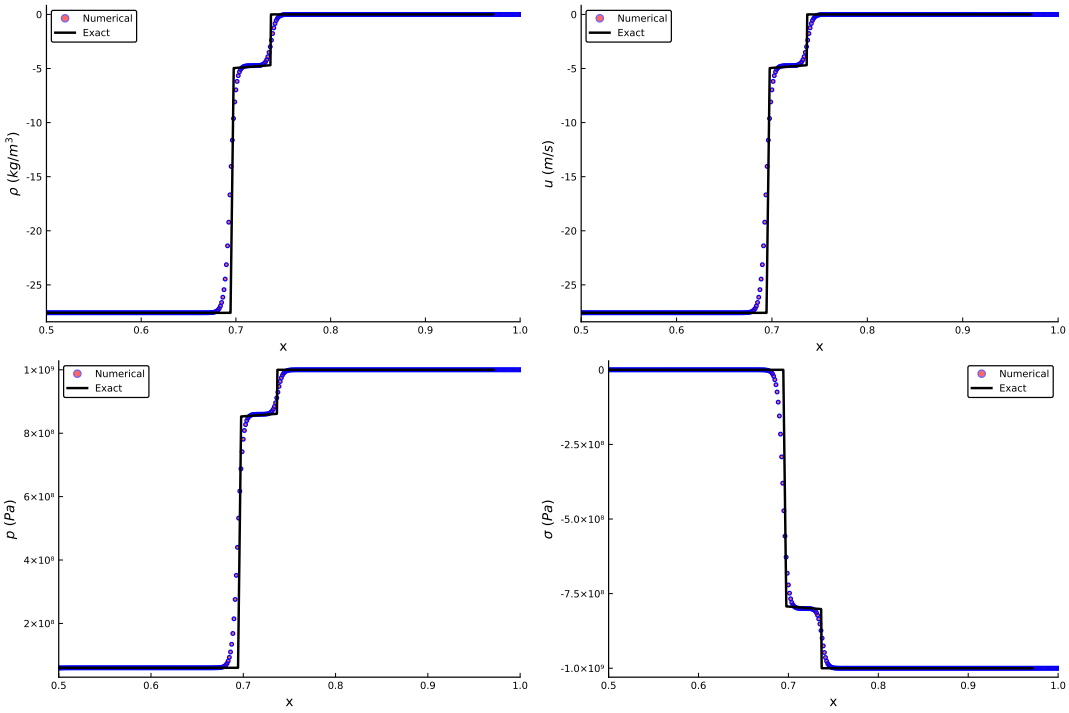

Figure 14: Comparison results for Test 11 with the structures of $R^E R^P$.

$$c_e(\rho_i) = \sqrt{a_0^2 \frac{\partial f}{\partial \eta}\left(\frac{\rho_i}{\rho_0}\right) + \frac{p(\rho_i)}{\rho_i^2}\rho_0\Gamma_0 - \frac{\rho_0}{\rho_i^2}\Gamma_0 s_{xx}(\rho_i) + \frac{4}{3}\frac{\mu}{\rho_i}}. \tag{A.4}$$

After finishing the evaluation of $p(\rho_i)$, we can evaluate $c_e(\rho_i)$ by using the same process as (A.2).